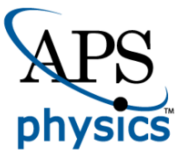

Fundamental Aspects of Parahydrogen Enhanced Low-Field Nuclear Magnetic Resonance

Johannes Colell, Pierre Türschmann, Stefan Glöggler, Philipp Schleker, Thomas Theis, Micah Ledbetter, Dmitry Budker, Alexander Pines, Bernhard Blümich, and Stephan Appelt

Phys. Rev. Lett. **110**, 137602 — Published 26 March 2013

DOI: 10.1103/PhysRevLett.110.137602

Fundamental Aspects of Parahydrogen Enhanced Low Field Nuclear Magnetic Resonance

Johannes Colell[1*]†, Pierre Türschmann[1]†, Stefan Glöggler[1], Philipp Schleker[1], Thomas Theis[2], Micah Ledbetter[3], Dmitry Budker[3], Alexander Pines[2], Bernhard Blümich[1], and Stephan Appelt[1,4]

[1]Institut für Technische Chemie und Makromolekulare Chemie, RWTH Aachen University, D-52074 Aachen, Germany.
[2]Department of Chemistry, University of California at Berkeley, Berkeley, California 94720-3220, USA
[3]Department of Physics, University of California at Berkeley, Berkeley, California 94720-7300, USA
[4]Zentralinstitut für Elektronik, Forschungszentrum Jülich, D-52425 Jülich, Germany.
† These authors contributed equally to this work.
*e-mail: johannes.colell@gmx.de

We report new phenomena in low-field ^{1}H nuclear magnetic resonance (NMR) spectroscopy using parahydrogen induced polarization (PHIP), enabling determination of chemical shift differences, $\delta\nu$, and the scalar coupling constant J. NMR experiments performed with thermal polarization in millitesla magnetic fields do not allow the determination of scalar coupling constants for homonuclear coupled spins in the inverse weak coupling regime ($\delta\nu < J$). We show here that low-field PHIP experiments in the inverse weak coupling regime enable the precise determination of $\delta\nu$ and J. Furthermore we experimentally prove that observed splittings are related to $\delta\nu$ in a non-linear way. Naturally abundant ^{13}C and ^{29}Si isotopes lead to heteronuclear J-coupled ^{1}H-multiplet lines with amplitudes significantly enhanced compared to the amplitudes for thermally prepolarized spins. PHIP-enhanced NMR in the millitesla regime allows to measure characteristic NMR parameters in a single scan using samples containing rare spins in natural abundance.

The established approach to liquid-state NMR spectroscopy in high fields is based on resolving NMR lines probing chemical shifts, J-coupling constants, and multiplicity. Those parameters are easily extracted from the spectra, because high-field experiments are typically performed in the weak coupling regime, where $\delta\nu >> J$ is valid. The clearly separated spectral lines allow identification of molecular structure. In the presence of rare spins additional heteronuclear J-coupled multiplets arise [1,2].

In the last decades various hyperpolarization technologies [3-6] and sensitive detection schemes [7-10] have rekindled the interest in low-field NMR. High resolution NMR spectroscopy with hyperpolarized molecules has been demonstrated in the earth's magnetic field and close to zero-field [10-13]. PHIP, where singlet state order (parahydrogen) is transferred into large observable nuclear polarization offers an attractive means of hyperpolarization [14-18]. NMR spectroscopy with hyperpolarized J-coupled spins at zero- and close to zero-field [19-21] has been demonstrated. In these cases the presence of rare spins (e.g. ^{15}N) in the molecule is required to yield observable transitions in J-coupled spin systems. Close to zero-field there are still ambiguity problems for molecules with more than two chemical groups and the chemical shift information is lost [22]. The drawbacks of low-

field NMR spectroscopy for pure ^{1}H spin-systems with thermal polarization are the low signal-to-noise ratio (*SNR*) and the loss of *J*-coupling and chemical shift information.

We show striking differences between the spectra obtained by PHIP and thermal prepolarization in low magnetic fields. In the following we detail how low-field PHIP spectra provide access to *J* and $\delta\nu$ in addition to benefitting from the inherent *SNR* enhancement that allows for single-shot acquisition of compounds containing rare spins in natural abundance.

Figure 1 illustrates the effect of magnetic field reduction and applied polarization method by comparison of simulated spectra, amplitude ratios and *SNR*. A *J*-coupled two- and three-spin system is used as a model, as experimental spectra shown here consist of superimposed spectra of two and three-spin systems. We introduce the dimensionless parameter $x = \delta\nu/J$, where $\delta\nu = \gamma B_0 (\delta_2 - \delta_1)$, γ is the gyromagnetic ratio of species I, B_0 is the static magnetic field and δ_1, δ_2 are the respective chemical shifts of spins I_1 and I_2. The upper three panels of Fig. 1a, b show numerical simulations of a *J*-coupled two-spin system (J = 8.5 Hz, $\delta_2 - \delta_1 = 2.4$ ppm, $I_1 = I_2 = 1/2$, $\pi/2$-excitation, linewidth = 0.7 Hz) for different values of x. With decreasing x, the inner two lines of the doublet of doublets merge and the outer transition lines vanish (Fig 1a). This is called "roof effect", because the intensities of the spectral line pattern mimics a roof with increasing tilt angle for decreasing x. The parameter x can thus be understood as an indicator for the relevance of the roof-effect for the spectrum of a compound at a given field strength, where for $x<<1$ the value of homonuclear coupling constants J can no longer be determined for thermally polarized samples. When applying PHIP with $\pi/2$-excitation (Fig. 1b), the spectra exhibit an antisymmetric structure with respect to the center-frequency $\nu_1 = \gamma B_0$. For small x, the inner two lines cancel out, while the outer two lines, separated by approximately $2J$, retain large amplitudes. The bottom panels of Fig. 1a, b show the spectra resulting from superposition of a *J*-coupled two-spin system (I_1I_2, 99%) and a three-spin system, I_1I_2S (S = 1/2, 1%), arising from the presence a rare spin in natural abundance. Using one heteronuclear coupling constant $J_{het} = 60$ Hz satellite peaks with a doublet-of-doublet structure (split by $J = 8.5$ Hz and by $J_{het} = 60$ Hz) arise for thermally polarized systems, with amplitudes three orders of magnitude smaller than the central line at ν_1. For PHIP satellite peaks are strongly enhanced relative to the suppressed central peak.

We define $R = |A_1|/|A_2| = |A_4|/|A_3|$, which is the amplitude ratio of transition lines with frequencies ν_4 and ν_1 to the lines at ν_3 and ν_2 to quantify the roof effect (see Fig. 1a, b). Figure 1c, where the analytically calculated R for thermal (dashed line) and parahydrogen polarization (solid and dotted line) is compared, reveals that R is highly dependent on the polarization method used, the field strength and the excitation pulse angle. In high field, where $x >> 1$, R converges to 1, independent of the polarization method. While for thermal polarization R decreases with decreasing x, R increases for PHIP. We call this suppression of inner transition line amplitudes (see Fig. 1b) inverse roof effect. As will be shown later, this has the benefit of allowing for the measurement of J and $\delta\nu$ in low magnetic fields. Although the inverse roof effect gets more pronounced with decreasing x, there is a limit to applicability of the phenomenon due to lower *SNR* at small x. Figure 1d shows the simulated *SNR* for the thermally prepolarized (dashed line) and parahydrogen polarized two-spin system (solid line $\pi/2$, dotted line $\pi/4$-excitation). For thermally prepolarized samples the *SNR* decreases

roughly as $\sqrt{x}$ for $x > 1$ and is proportional to x for $x < 1$, whereas *SNR* for PHIP also depends on the excitation pulse angle. PHIP after π/4-excitation yields best *SNR* in high fields, while for a π/2-pulse the maximum is at $x = 2\sqrt{2}$. The absolute values for the *SNR* were determined by comparing the signal of our sample, thermally prepolarized at 2T, to the PHIP signal of the two relevant protons. The existence of a maximum in *SNR* can be explained by the initial density matrix of a singlet evolving into a state with symmetry broken by $\delta\nu$. After an excitation pulse with tip angle θ in the x-direction the density matrix is [23,24]

$$\rho_{para}^{av}(\theta) = sin\,\theta\,cos\,\theta\left\{\frac{1}{x^2+1} - 1\right\}\left(I_{1y}I_{2z} + I_{1z}I_{2y}\right) + sin\,\theta\left\{\frac{x}{2(1+x^2)}\right\}\left(I_{2y} - I_{1y}\right), \qquad (1)$$

where I_{1y}, I_{1z} and I_{2y}, I_{2z} are the operators for the y and z components of spins I_1 and I_2. After π/2-excitation the observed NMR signal depends only on the term $\{x/(2(1+x^2))\}\left(I_{2y} - I1y\right.$, which is responsible for the maximum in the *SNR*. The negative sign results in the anti-symmetric peak patterns in the simulations.

A consequence of the inverse roof effect for PHIP at $x < 1$ is that the measurement of the lines at ν_4 and ν_1 allows determining J and $\delta\nu$ when measuring at different values of x. Evaluation of the energy eigenvalues and corresponding transition frequencies of the *J*-coupled two-spin system shows that for $x < 1$ the frequency difference $\nu_4 - \nu_1$ as a function of x is given by [26]

$$\nu_4 - \nu_1 = 2J\,[1 + x^2/4 - x^4/16 + \cdots]. \qquad (2)$$

While this effect cannot be measured in high field (10T) the quadratic splitting is experimentally observable in low field ($x < 0.1$).

In order to verify Fig. 1 and the validity of Eq. (2) the ynol-ether 1-(*tert*-butyldiphenylsilyl)-2-(ethoxy)ethyne, in the following referred to as (**1**), was synthesized, which forms a *J*-coupled two-spin system after reaction with parahydrogen *p*-H_2 (Fig. 2b). The structure of the compound is R_1-C_a≡C_b-R_2, where R_1 is an electron donating and R_2 an electron drawing group, resulting in a large chemical shift difference between protons H_a-H_b after hydrogenation [25]. The isotopomers are 93.3% R_1-C_a ≡ C_b-R_2, 1% R_1-$^{13}C_a$ ≡ C_b-R_2, 1% R_1-C_a ≡ $^{13}C_b$-R_2 as well as 4.7% TBDP^{29}Si-C_a ≡ C_b -R_2. After hydrogenation, the resulting enol ether, in the following referred to as (**2**), consists of one two-spin system (H_a-H_b) and three different three-spin systems (^{29}Si-H_a-H_b, $^{13}C_a$-H_a-H_b, H_a-$^{13}C_b$-H_b).

Low-field measurements were performed on a home built low-field NMR spectrometer (noise close to Johnson-noise limit) using a solenoid with four shimming coils (0.7 ppm/cm^3) supplied by a current source with sub-ppm stability (Fig. 2a). The probe is part of a shuttle system used to transport the sample to the center of the magnet. PHIP experiments were performed using a Bruker BPHG090 Parahydrogen Generator (93 % parahydrogen). Data

were acquired for 10 seconds with a sampling period of 100 µs. 1.2 mg of the Rhodium catalyst [1,4-Bis(diphenylphosphino)butane](1,5-cycloocta-diene)rhodium(I)tetrafluoroborate were dissolved in 320 µL anhydrous acetone-d_6. 40 µL of pure R_1-C_a≡C_b-R_2 were added to the mixture. The sample was connected to the parahydrogen supply with a hydrogen pressure of 5 bar. After shaking in the stray field of the magnet (5 G) for 10 seconds the sample was transferred into the homogeneous field B_0 (3 s transfer time), where the spin system evolves into the density matrix defined by Eq. (1). $\delta_{Ha} - \delta_{Hb} = 2.4$ ppm and $^3J_{HaHb} = 8.48$ Hz for compound (**2**) was also determined in high field (400 MHz). Measurements with thermal prepolarization were performed by polarizing the sample at $B_P = 2$ T and transferring the sample into the probehead.

Figure 2c shows the ^{1}H free induction decay (FID, 500 kHz, π/2 pulse) of a thermally polarized sample of (**2**) with corresponding spectrum in Fig. 2d. The spectrum consists of two overlapping broad lines (~ 3 Hz linewidth) with peak maxima separated by 3 Hz (6 ppm). The main contributions to the spectral pattern result from the overlapping lines of the aliphatic protons (*t*-butyl and ethoxy group) and of the aromatic and olefinic protons (phenyl and ethene groups), where the chemical shift difference between the mean values of the ^{1}H chemical shifts of similar groups is 6 ppm.

PHIP spectra of (**2**) have higher information content than thermally polarized spectra regarding the catalytically added protons and rare spins in their vicinity. Figure 3a shows the ^{1}H-FID of a PHIP experiment performed at 500 kHz ($x = 0.141$) with π/2-excitation with 500 times higher *SNR* than the thermally polarized experiment. The spectrum in Fig. 3b is antisymmetric with respect to its center (average linewidth ~ 0.7 Hz). Red arrows indicate the outer transition lines of the H_a-H_b two-spin system separated by $\nu_4 - \nu_1 = (17.052 \pm 0.008)$ Hz. The simulated spectrum in Fig. 3c is calculated with a generalized version [26] of the three-spin density matrix described in Ref. [27] and is in good agreement with the experimental results (Fig. 3b). This shows that the measurement is a superposition of the spectra of all isotopomers, thereby containing information about the chemical shift difference between H_a and H_b, and homo- and heteronuclear *J*-coupling constants between H_a-H_b, H_a-$^{13}C_a$, H_b-$^{13}C_b$, H_b-^{29}Si and H_a-^{29}Si.

The ^{13}C isotopomers result in two doublets of doublets split by two heteronuclear coupling constants $^1J_{HaCa} = 140.74$ Hz, $^1J_{HbCb} = 177.92$ Hz and by the homonuclear coupling $^3J_{HaHb} = 8.48$ Hz. The amplitudes and the frequency separation of the doublet of doublets, split by the $^2J_{HaCb}$ and $^2J_{HbCa}$, are small and masked by the large amplitudes of the *J*-coupled ^{29}Si-H_a-H_b lines. The inset in Fig. 3b contains four times averaged ^{1}H-spectra of the ^{13}C isotopomers for clarity. The simulated spectrum of the three-spin system ^{29}Si-H_a-H_b ($^3J_{HbSi} = 11$ Hz, $^2J_{HaSi} = -0.5$ Hz, and $^3J_{HaHb} = 8.48$ Hz) shows an antisymmetric pair of four lines (Fig. 3c), which could not all be resolved in the experimental spectrum in Fig. 3b. The spectrum in Fig. 3d (166 kHz ^{1}H frequency) essentially shows the same features as Fig. 3b, but the antisymmetric pair of four lines is fully resolved. In full accordance with the *SNR* calculations (Fig. 1d) the line amplitudes at ν_1, ν_4 are smaller.

The lines marked by arrows in Figs. 3b and 3d encode the chemical shift difference $\delta\nu = \gamma_H B_0(\delta_{Ha} - \delta_{Hb})$. Evaluating the line separation $\nu_4 - \nu_1$ at 500 kHz with the truncated

expression of Eq. (2) ($J = {}^3J_{\mathrm{HaHb}}$) results in $x = 0.141$. This corresponds to $\delta\nu = 1.2$ Hz and $\delta_{\mathrm{Ha}} - \delta_{\mathrm{Hb}} = 2.4$ ppm, identical to the chemical shift difference measured at high field. Eq. (2) was verified by measuring the line separation at different values of x (Fig. 4a). The theoretical prediction according to Eq. (2) (solid line) is in good agreement with the measured data (squares). Error bars indicate the standard error of the center-frequency over five measurements, where the experimental error is more significant at lower magnetic field strengths due to SNR restrictions and field fluctuations.The value for $\nu_4 - \nu_1$ at $x = 0$ is given by $2\ {}^3J_{\mathrm{HaHb}} = 16.96$ Hz, which can be measured in high field or be obtained from the spectrum in Fig. 4b by evaluating the line splitting caused by ${}^3J_{\mathrm{HaHb}}$ in the structure of the ^{13}C satellites.

Figure 4b shows a PHIP-enhanced spectrum obtained after one single π/4-excitation at 500 kHz, showing that spectral features are highly dependent on θ. Heteronuclear coupled ^{1}H-^{13}C lines exhibit clear anti-phase structure with amplitudes three times larger than the ^{1}H-^{13}C multiplet lines in Fig. 3b. For π/4-excitation the amplitudes can be explained by a symmetry breaking mechanism involving both chemical shift and heteronuclear *J*-couplings [26]. The chemical shift difference $\delta\nu = 1.2$ Hz can also be extracted from Fig. 4b. The center-frequency of the outer anti-phase doublet-of-doublet lines (spaced by ${}^1J_{\mathrm{HbCb}} = 177.92$ Hz) is displaced relative to the inner doublet-of-doublet lines (spaced by ${}^1J_{\mathrm{HaCa}} = 140.74$ Hz) by exactly $\delta\nu = 1.2$ Hz.

In conclusion we have demonstrated several fundamental differences between thermally prepolarized and PHIP ^{1}H NMR spectroscopy at low magnetic field: The larger *SNR* and the inverse roof effect of the parahydrogen polarized spins allow for the measurement of the homonuclear *J*-coupling and nonlinear splittings encoding the chemical shift difference even in the absence of heteronuclei. Furthermore if rare spins are present the amplitudes of the heteronuclear *J*-coupled multiplet lines are significantly enhanced. For future work, the analysis of homonuclear systems needs to be extended to include spin-systems with more than two spins. The combination of a low cost hyperpolarization technique like PHIP with mobile low-field NMR yields the same information about the investigated PHIP-enhanced molecular group as high field PHIP-NMR experiments. Investigation of the order transfer from the pure initial spin-state offered by parahydrogen combined with the portable NMR hardware could open applications for the development of new NMR quantum computers [28]. The results can be seen as a further milestone for low-field NMR spectroscopy and will open the way for new applications in material science, spin physics and mobile chemical analytics.

Corresponding author: Johannes Colell, mailto: johannes.colell@gmx.de

Acknowledgements

The authors gratefully acknowledge excellent technical assistance from U. Sieling, J. Schmitz, S. van Waasen, G. d´Orsaneo, A. Schwaitzer, H. Glückler from the Forschungszentrum Jülich, J. Klankermayer from the RWTH Aachen University for helpful discussions, J. M. Tyburn, J. Lohmann and D. Kilgour from Bruker Biospin GmbH for technical advice and support of the Bruker BPHG090 Parahydrogen Generator, and to Hero Faierstein from VISHAY for the supply of special ultra-precision shunt resistors.
SA gratefully acknowledges funding by the Excellence Initiative of the German federal and state governments. MPL and DB gratefully acknowledge the support of the National Science Foundation under Grant CHE-0957655. This research was supported in part by the U.S. Department of Energy, Office of Basic Energy Sciences, Division of Materials Sciences and Engineering under Contract No. DE-AC02-05CH11231 (TT and AP).

Additional information

The authors declare that they have no competing financial interests. The exact analytical expressions, the quantum mechanical calculations, details of the numerical simulations, and the initial density matrices will be published elsewhere.

References

1. R. R. Ernst, G. Bodenhausen and A. Wokaun, Principles of Nuclear Magnetic Resonance in One and Two Dimensions (Clarendon Press, Oxford, UK, 1987).
2. H. Günther, NMR spectroscopy (John Wiley & Sons, 1973).
3. T. G. Walker and W. Happer, Rev. Mod. Phys. **69**, 629 (1997).
4. S. Appelt, A. Ben-Amar Baranga, C. J. Erickson, M. V. Romalis, A. R. Young, and W. Happer, Phys. Rev. A **58**, 1412 (1998).
5. T. R. Carver, and C. P. Slichter, Phys. Rev. **102**, 975 (1956).
6. G. Navon, Y. Q. Song, T. Room, S. Appelt, R. E. Taylor, and A. Pines, Science **271**, 1848 (1996).
7. I. M. Savukov, and M. V. Romalis, Phys. Rev. Lett. **94**, 123001 (2005).
8. Y. S. Greenberg, Rev. Mod. Phys. **70**, 175 (1998).
9. M. Poggio, C. L. Degen, Nanotechnology **21**, 342001 (2010).
10. R. McDermott, A. H. Trabesinger, M. Mueck, E. L. Hahn, A. Pines, and J. Clarke, Science **295**, 2247 (2002).
11. S. Appelt, F. W. Häsing, H. Kühn, J. Perlo, and B. Blümich, Physical Review Letters **94**, 197602 (2005).
12. S. Appelt, H. Kühn, F. W. Häsing, and B. Blümich, Nat. Phys. **2**, 105 (2006).
13. B. C. Hamans, A. Andreychenko, A. Heerschap, S. S. Wijmenga, and M. Tessari, Journal of Magnetic Resonance **212**, 224 (2011).
14. S. Aime, D. Canet, W. Dastru, R. Gobetto, F. Reineri, and A. Viale, J. Phys. Chem. A **105,** 6305 (2001).

15. L. S. Bouchard, S. R. Burt, M. S. Anwar, K. V. Kovtunov, I. V. Koptyug, A. Pines, Science **319**, 442 (2008).
16. K. V. Kovtunov, I. E. Beck, V. I. Bukhtiyarov, and I. V. Koptyug, Angew. Chem. **120**, 1514 (2008).
17. C. R. Bowers, and D. P. Weitekamp, Phys. Rev. Lett. **57,** 2645 (1986).
18. R. W. Adams, J. A. Aguilar, K. D. Atkinson, M. J. Cowley, P. I. P. Elliott, S. B. Duckett, G. G. R. Green, I. G. Khazal, J. Lopez-Serrano, and D. C. Williamson, Science **323**, 1708 (2009).
19. T. Theis, P. J. Ganssle, G. Kervern, S. Knappe, J. Kitching, M. P. Ledbetter, D. Budker, and A. Pines, Nat. Phys. **7**, 571 (2011).
20. T. Theis, M. P. Ledbetter, G. Kevern, J. W. Blanchard, P. J. Ganssle, M. C. Butler, S. D. Shin, D. Budker, and A. Pines, Journal of American Chemical Society **134**, 3987 (2012).
21. M. P. Ledbetter, T. Theis, J. W. Blanchard, H. Ring, P. J. Ganssle, S. Appelt, B. Blümich, A. Pines, and D. Budker, Phys. Rev. Lett. **107**, 107601 (2011).
22. S. Appelt, F. W. Häsing, U. Sieling, A. Gordji-Nejad, S. Glöggler, and B. Blümich, Phys. Rev. A. **81**, 023420(11) (2010).
23. J. Natterer, and J. Bargon, Prog. Nucl. Magn. Reson. Spectrosc. **31**, 293 (1997).
24. D. Canet, C. Aroulanda, P. Mutzenhardt, S. Aime, R. Gobetto, and F. Reineri, Concepts Magn. Reson. Part A **28A** 321 (2006).
25. F. Longpré, N. Rusu, M. Larouche, R. Hanna, and B. Daoust, Can. Journal of Chemistry **86**, 970 (1999).
26. Manuscript in Preparation
27. J. Natterer, O. Schedletzky, J. Barkemeyer, J. Bargon, and S. J. Glaser, J. Magn. Reson. **133**, 92 (1998).
28. M. S. Anwar, J. A. Jones, D. Blazina, S. B. Duckett, H. A. Carteret, Phys. Rev. A **70**, 032324 (2004).

Figure legends:

FIG. 1 Fundamental differences between thermally and PHIP prepolarized NMR. **a**, Simulated NMR spectra ($\pi/2$-excitation) of a thermally prepolarized *J*-coupled two-spin I_1-I_2-system at different fields (x = 6, 1, 0.15) and a three-spin system S-I_1-I_2 (fourth panel) using one heteronuclear coupling constant $J_{S\text{-}I1} = J_{\text{het}}$ = 60 Hz. **b**, same as **a** but with PHIP. **c**, Ratio $R = |A_4|/|A_3|$ as a function of $x = \delta\upsilon/J$ for thermally prepolarized spins (dashed line), PHIP after $\pi/4$- (dotted line) and $\pi/2$-excitation (solid line). The discontinuity for π/4-excitation is caused by a change in sign of the amplitude of the inner transition lines [26]. **d**, Theoretical *SNR* of the I_1-I_2 spin-system as a function of x for thermal prepolarization at 2 T (dashed line) and PHIP after $\pi/4$- (dotted line) and $\pi/2$-excitation (solid line).

FIG. 2 Experimental setup and procedure. **a**, The nuclear spins of a liquid sample are either prepolarized by a 2 T Halbach magnet or by PHIP. After $\pi/2$- or $\pi/4$-excitation the free induction decay (FID) of the nuclear spins is acquired and processed. **b**, Reaction of 1-(*tert*-butyldiphenylsilyl)-2-(ethoxy)ethyne (**1**) to (**2**) in the presence of a Rhodium (Rh) catalyst and 5 bar p-H_2. **c**, Single scan ^{1}H FID of 40 µl of (**2**) after prepolarization at 2 T and $\pi/2$-excitation. **d**, Fourier transformed spectrum of **c** measured at 500 kHz shows two broad lines.

FIG. 3 ^{1}H-low-field NMR of a parahydrogen polarized two-spin system. **a**, PHIP ^{1}H FID at 500 kHz of 1-(*tert*-butyldiphenylsilyl)-2-(ethoxy)ethen measured at 12 mT with $\pi/2$-excitation. **b**, spectrum of **a** (linewidth ~ 0.7 Hz). **c**, Simulated spectrum referring to Fig. 3**b**. Red arrows indicate line positions of the I_1-I_2 system, other lines correspond to the hetero- and homonuclear *J*-coupled systems S-I_1-I_2. **d**, same as **b** but at measured 166 kHz ^{1}H-frequency.

FIG. 4 Chemical shift of p-H_2 polarized two- and three-spin systems. **a**, Frequency difference $\upsilon_4 - \upsilon_1$ measured at 166, 335, 500 and 666 kHz ^{1}H-frequency (squares). Axis on top denotes the corresponding values of x. Solid line represents $\upsilon_4 - \upsilon_1 = 2\ {}^3J_{\text{HaHb}}(1 + 0.25\ x2$ with ${}^3J_{\text{HaHb}}$ = 8.48 Hz. **b**, Single-scan ^{1}H-spectrum of 40 μL PHIP hyperpolarized 1-(*tert*-butyldiphenylsilyl)-2-ethoxyethen measured at 500 kHz with $\pi/4$-excitation.

(a)

(b)

Spectral Intensity

ν_1 ν_2 ν_3 ν_4

$I_1 I_2$

$x = 6$

$x = 1$

$x = 0.15$

x100

x500

$I_1 I_2$ with 1% S

x25

Frequency

Frequency

(c)

Intensity Ratio R

10^{4} 10^{2} 10^{0} 10^{-2} 10^{-4}

10^{-2} 10^{-1} 10^{0} 10^{1} 10^{2}

x

(d)

SNR

10^{4} 10^{2} 10^{0} 10^{-2}

10^{-2} 10^{-1} 10^{0} 10^{1} 10^{2}

x

(a)

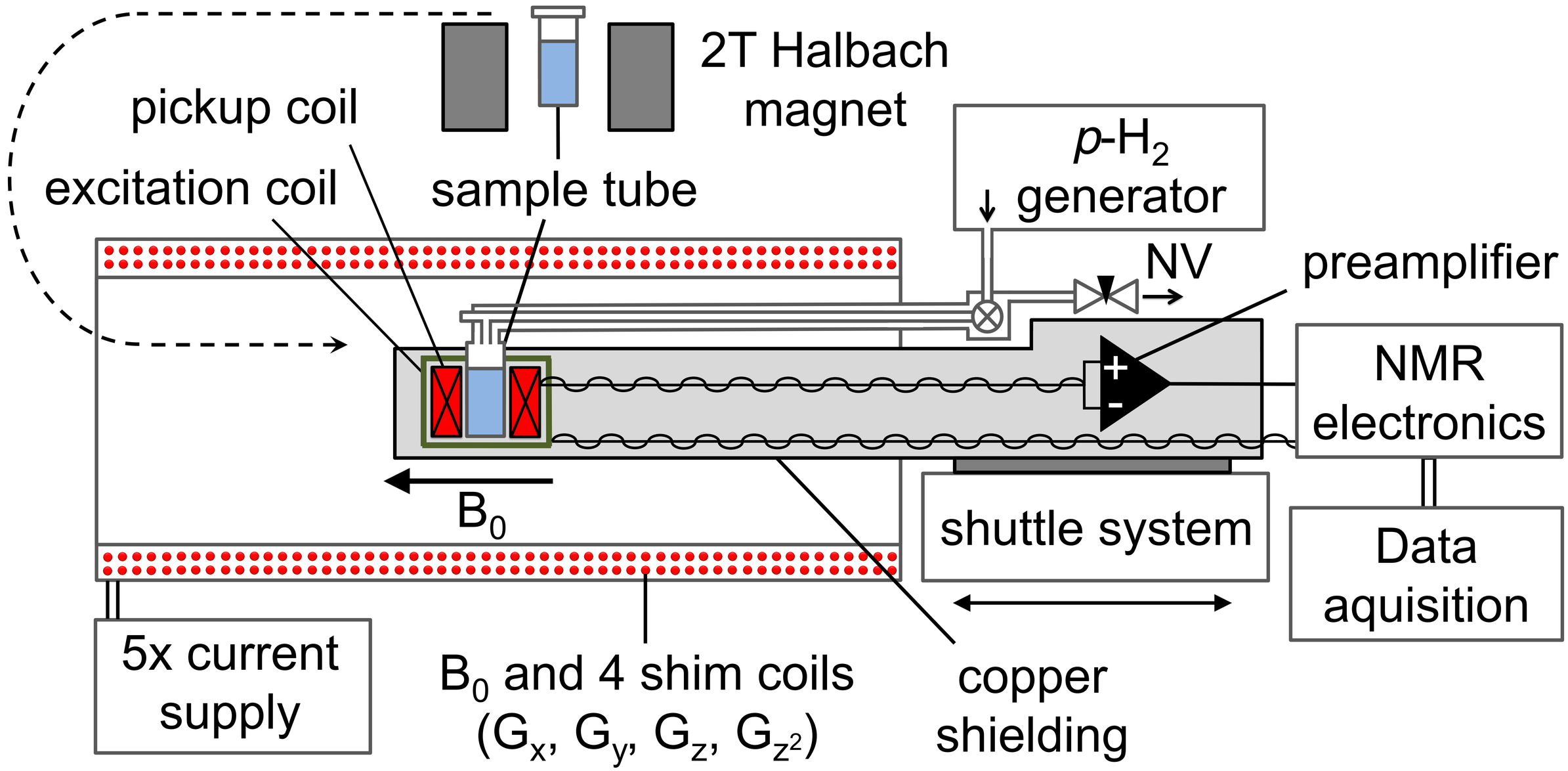
2T Halbach magnet
pickup coil
excitation coil
sample tube
p-H2 generator
NV
preamplifier
NMR electronics
Data aquisition
shuttle system
B0
5x current supply
B0 and 4 shim coils (Gx, Gy, Gz, Gz2)
copper shielding

(b)

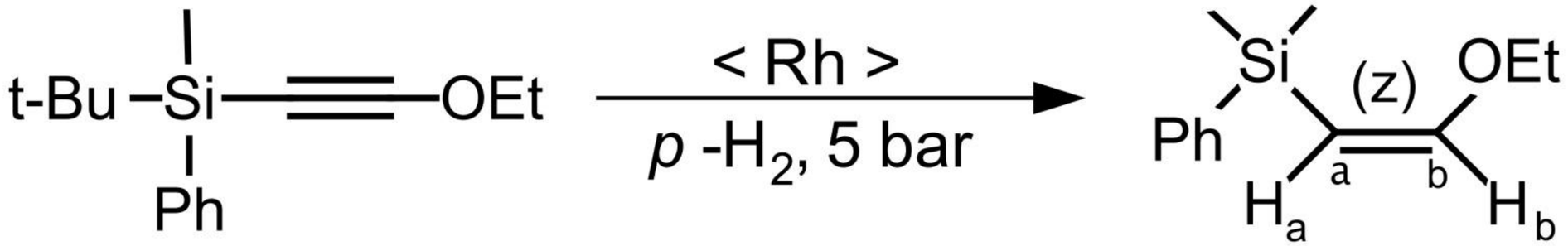
t-Bu
Si
Ph
OEt
< Rh >
p -H2, 5 bar
Si
Ph
(z)
OEt
a
b
Ha
Hb

(1) (2)

(c)

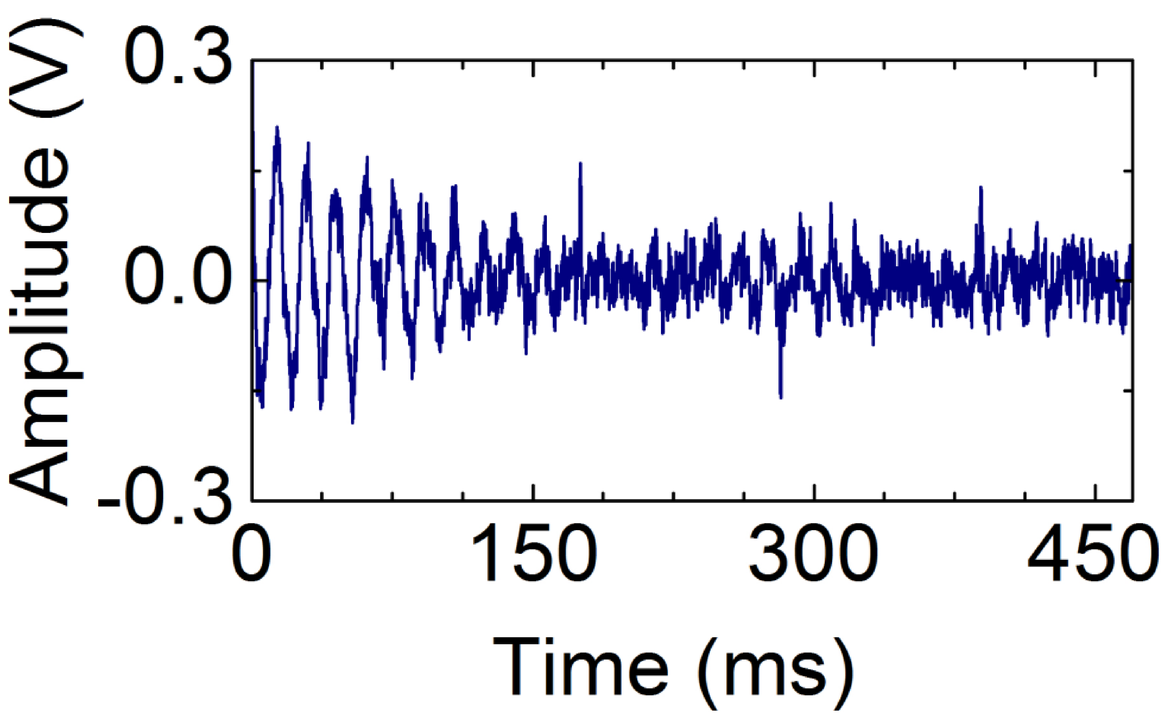
Amplitude (V)
0.3
0.0
-0.3
0
150
300
450
Time (ms)

d

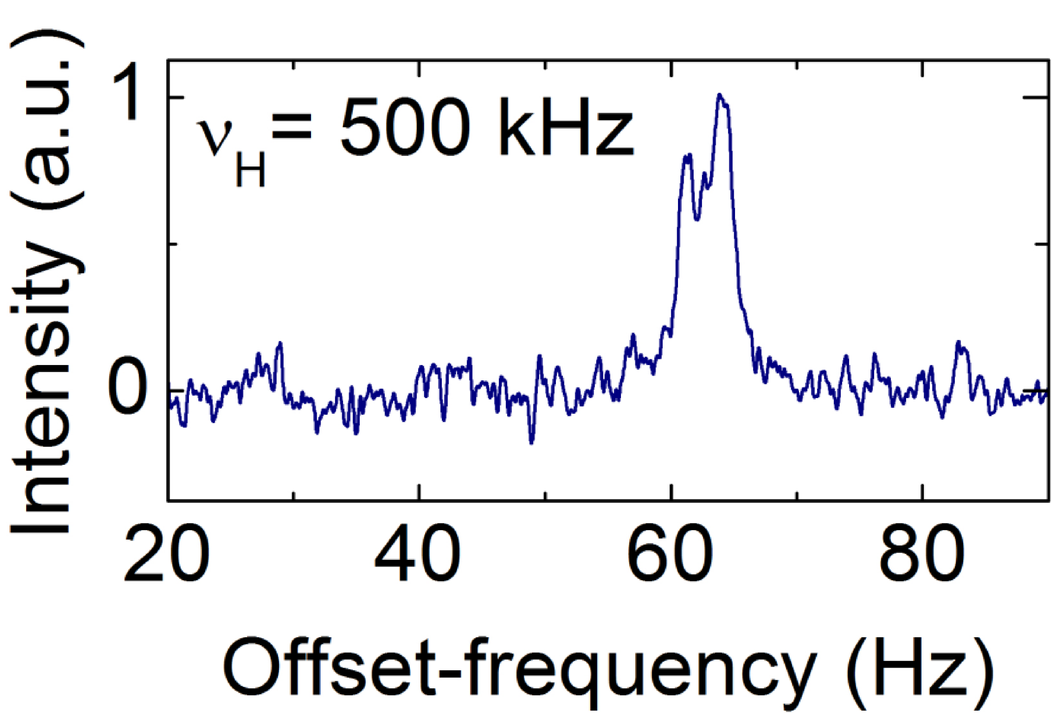
Intensity (a.u.)
1
0
νH = 500 kHz
20
40
60
80
Offset-frequency (Hz)

(a)

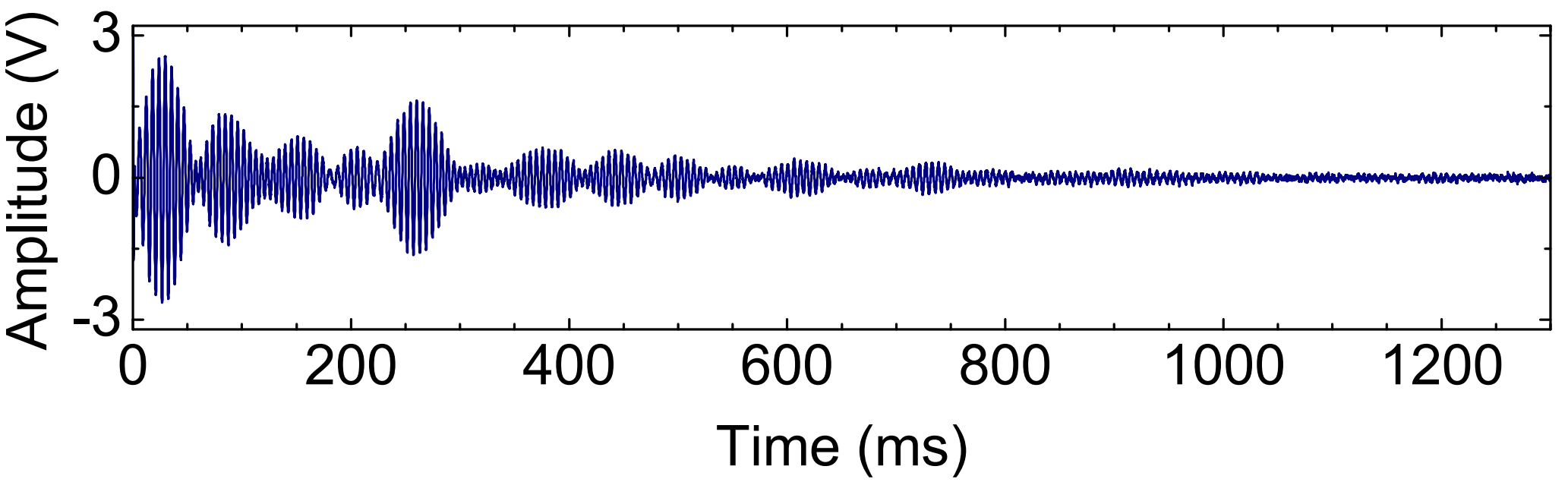
Amplitude (V)
3
0
-3
0
200
400
600
800
1000
1200
Time (ms)

(b)

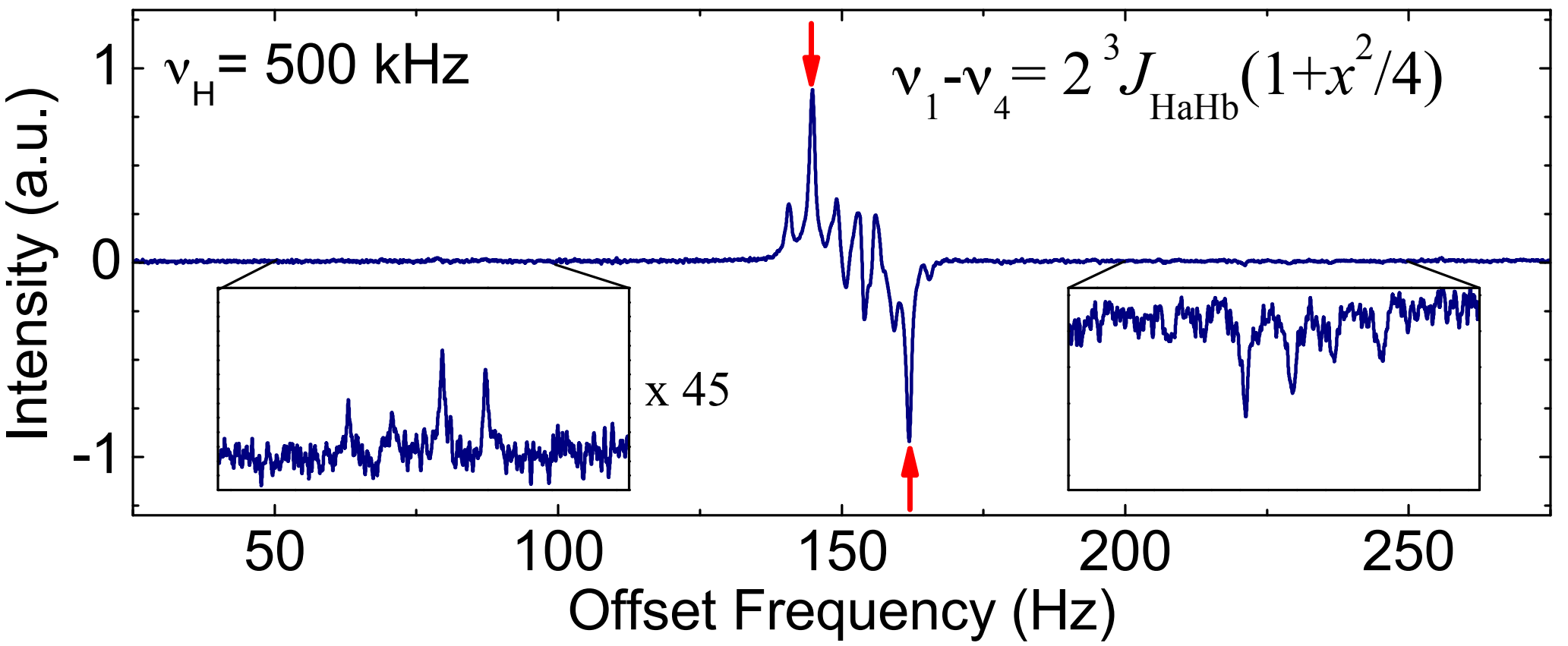
ν_H= 500 kHz
ν_1-ν_4 = $2\,{}^3J_{\mathrm{HaHb}}(1+x^2/4)$
Intensity (a.u.)
1
0
-1
x 45
50
100
150
200
250
Offset Frequency (Hz)

(c)

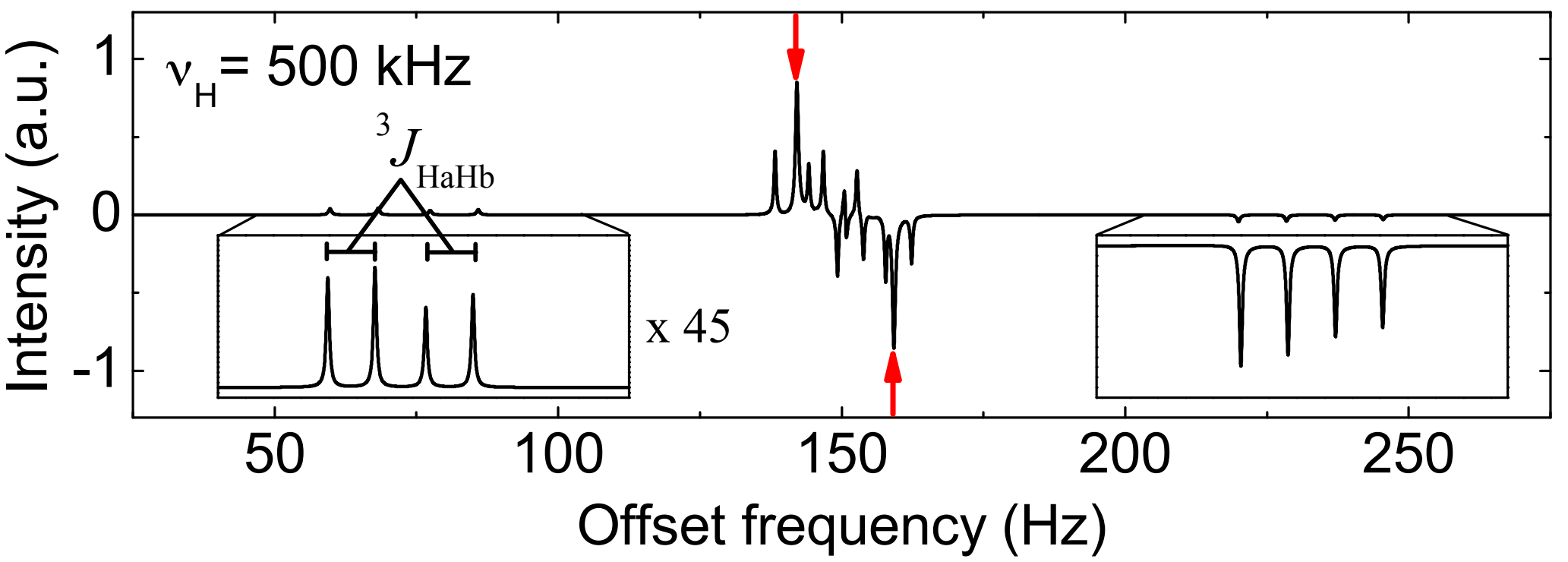
ν_H= 500 kHz
${}^3J_{\mathrm{HaHb}}$
Intensity (a.u.)
1
0
-1
x 45
50
100
150
200
250
Offset frequency (Hz)

(d)

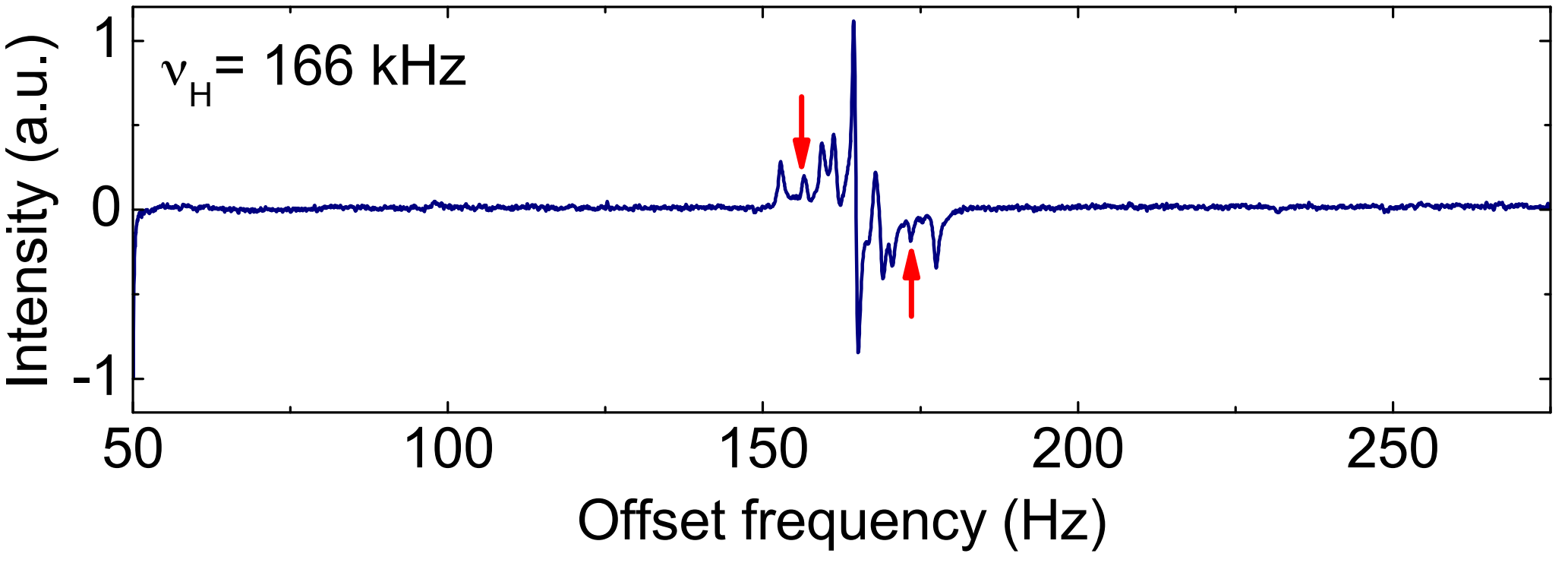
ν_H= 166 kHz
Intensity (a.u.)
1
0
-1
50
100
150
200
250
Offset frequency (Hz)

(a)

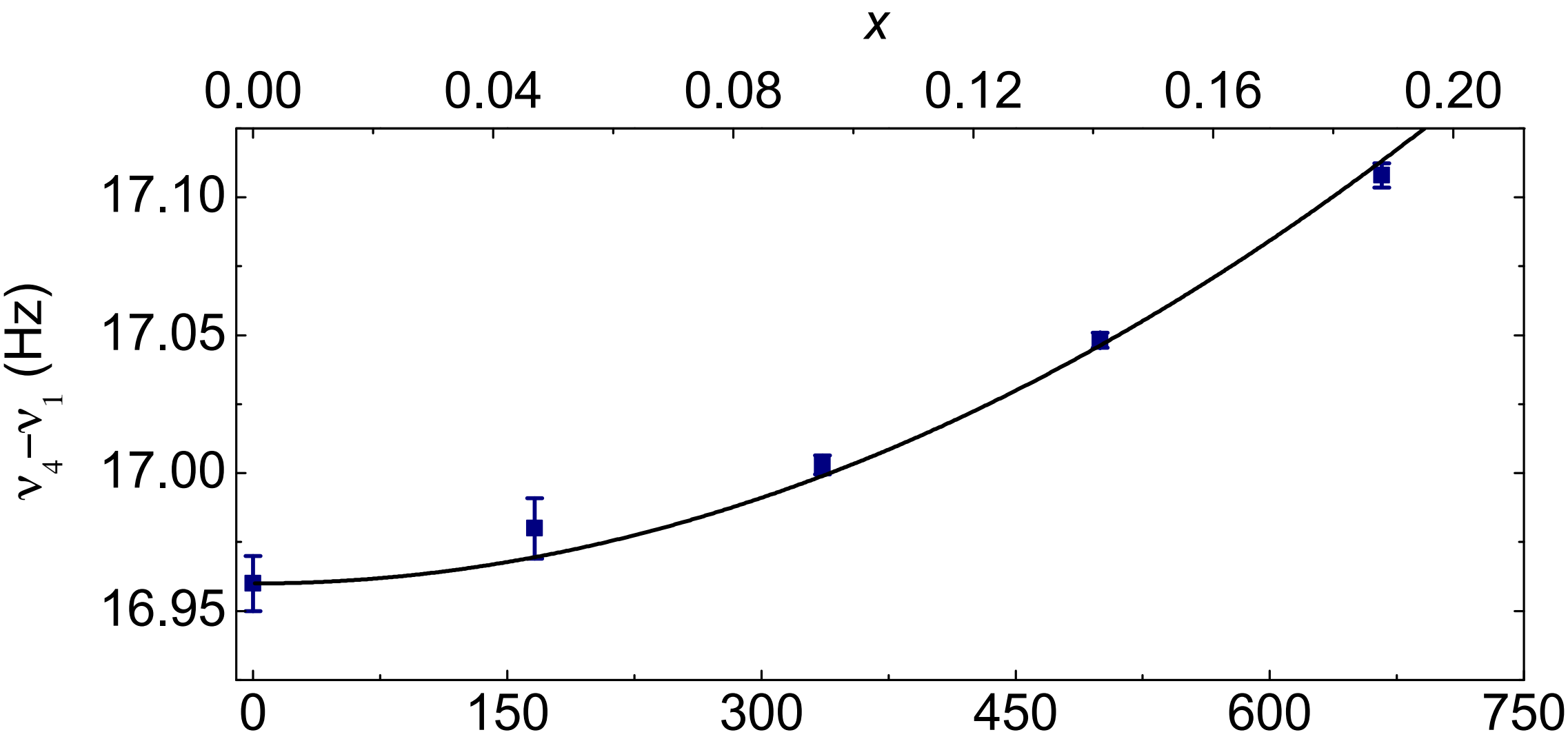
x
0.00
0.04
0.08
0.12
0.16
0.20
17.10
17.05
17.00
16.95
$\nu_4 - \nu_1$ (Hz)
0
150
300
450
600
750

(b)

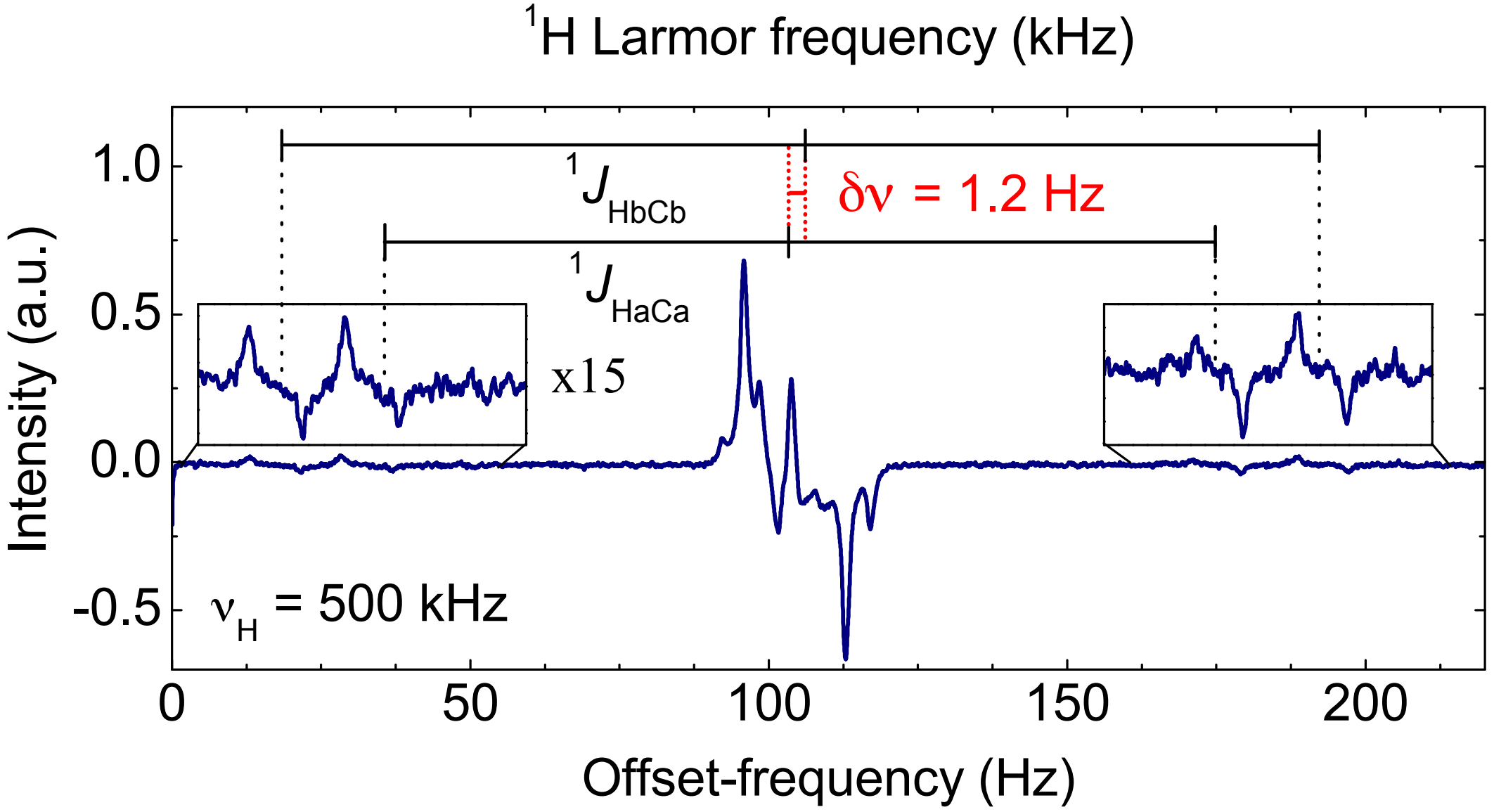
^{1}H Larmor frequency (kHz)
1.0
0.5
0.0
-0.5
Intensity (a.u.)
$^1J_{HbCb}$
$^1J_{HaCa}$
δν = 1.2 Hz
x15
ν_H = 500 kHz
0
50
100
150
200
Offset-frequency (Hz)